Article

Not peer-reviewed version

Synthesis and Antibacterial Evaluation of Silver-Coated Magnetic Iron Oxide/Activated Carbon Nanoparticles Derived from Hibiscus esculentus

Muslum Gunes , Erdal Ertaş * , Seyhmus Tumur , Parvin Zulfugarova , Fidan Nuriyeva , Taras Kavetskyy * , Yuliia Kukhazh , Pavlo Grozdov , Ondrej Šauša , Oleh Smutok * , Dashgin Ganbarov , Arnold Kiv

Posted Date: 16 May 2025

doi: 10.20944/preprints202505.1245.v1

Keywords: Magnetic nanoparticles; activated carbon; Hibiscus esculentus; silver coating; antimicrobial properties

 doi:10.20944/preprints202505.1245.v1

Article

Synthesis and Antibacterial Evaluation of Silver-Coated Magnetic Iron Oxide/Activated Carbon Nanoparticles Derived from *Hibiscus esculentus*

Müslüm Güneş [1], Erdal Ertaş [2,*], Seyhmus Tumur [3], Parvin Zulfugarova [4], Fidan Nuriyeva [5], Taras Kavetskyy [6,7,8,*], Yuliia Kukhazh [6], Pavlo Grozdov [6], Ondrej Šauša [7,9], Oleh Smutok [10,*], Dashgin Ganbarov [11] and Arnold Kiv [8,12]

1. SBU Diyarbakir Gazi Yasargil Education and Research Hospital, 21280 Diyarbakır, Turkey
2. Department of Food Technology, Vocational School of Technical Sciences, Batman University, 72000 Batman, Turkey
3. Department of Civil Engineering, Dicle University, 21280 Diyarbakir, Turkey
4. Department of Zoology and Physiology, Faculty of Biology, Baku State University, AZ1148 Baku, Azerbaijan
5. Department of Computer Science, Faculty of Science, Dokuz Eylul University, 35390 Buca, Izmiz, Turkey
6. Drohobych Ivan Franko State Pedagogical University, 82100 Drohobych, Ukraine
7. Institute of Physics, Slovak Academy of Sciences, 84511 Bratislava, Slovakia
8. South Ukrainian National Pedagogical University named after K.D. Ushynsky, 65020 Odesa, Ukraine
9. Department of Nuclear Chemistry, FNS, Comenius University, 84215 Bratislava, Slovakia
10. Department of Chemistry and Biochemistry, Clarkson University, 13699 Potsdam, NY, USA
11. Nakhchivan State University, AZ7012 Nakhchivan, Azerbaijan
12. Department of Materials Engineering, Ben-Gurion University of the Negev, 84105 Beer-Sheva, Israel

* Correspondence: erdalertas21@gmail.com (E.E.); kavetskyy@yahoo.com (T.K.); osmutok@clarkson.edu (O.S.)

Abstract: The rise of antimicrobial resistance due to the indiscriminate use of antibiotics has become a global health crisis, contributing to millions of deaths each year. Given the limitations and side effects associated with current antibiotics, there is an urgent need to develop alternative antimicrobial agents that are both safe and effective. In this study, magnetic iron oxide nanoparticles (MIONPs) were synthesized via a chemical co-precipitation technique involving the simultaneous precipitation of Fe^{2+} and Fe^{3+} ions in an alkaline medium and supported on activated carbon (AC) derived from *Hibiscus esculentus* (HE) fruits, resulting in the formation of MIONPs/HEAC nanocomposites. To enhance their antimicrobial activity, these nanocomposites were further modified with a silver coating via the chemical reduction of silver ions using sodium borohydride, producing MIONPs/HEAC@Ag. The structure and properties of the nanoparticles were analyzed using various techniques. SEM and EDX were used to observe morphology and elemental makeup. DLS and zeta potential measured the size and surface charge. FTIR identified functional groups, and XRD determined crystallinity. The antibacterial activity of MIONPs/HEAC and MIONPs/HEAC@Ag was evaluated against bacterial strains of *Escherichia coli* and *Staphylococcus aureus*. The uncoated MIONPs/HEAC showed no antibacterial effect, whereas the MIONPs/HEAC@Ag exhibited significant antibacterial activity, with inhibition zones measuring 11.50 mm for *E. coli* and 13.00 mm for *S. aureus*. These results highlight the potential of MIONPs/HEAC@Ag nanocomposites as promising candidates for biomedical applications, particularly in addressing infections caused by antibiotic-resistant bacteria.

Keywords: Magnetic nanoparticles; activated carbon; *Hibiscus esculentus*; silver coating; antimicrobial properties

1. Introduction

Nanoscience and nanotechnology are broad, multidisciplinary fields that involve the creation, investigation, and utilization of materials and systems with dimensions typically between 1 and 100

 doi:10.20944/preprints202505.1245.v1

nanometers, where unique phenomena often emerge due to the scale. Nanoparticles, due to their diminutive size, exhibit distinctive properties and functionalities, including enhanced physical and chemical stability, thermal resistance, and unique electrical, magnetic, optical, and biological characteristics. These properties enable nanoparticles to function as integral components with novel levels of activity at the nanoscale [1–3]. In comparison to their bulk counterparts of identical composition, nanoparticles display superior enzymatic reactivity, catalytic performance, chemical and biological activity, permeability, and quantum mechanical behaviors. These enhanced properties are primarily attributed to their increased surface area-to-volume ratio and improved mass transfer dynamics. Owing to these attributes, nanoparticles have garnered significant attention across a range of fields, particularly in biomedicine, where they are extensively studied for applications in disease diagnosis and therapeutic interventions. In recent years, considerable research efforts have been devoted to reducing materials with well-defined structures and compositions to the nanoscale in order to intentionally alter their chemical and physical properties, thereby enabling the development of advanced functional materials for targeted applications [4,5].

Metallic nanoparticles, among the most fundamental nanoscale structures, have found extensive applications across various industrial sectors. In recent years, a refined nomenclature has emerged within the field of nanotechnology to better classify and describe these particles. Metallic nanoparticles, which are synthesized using methods tailored for nanoparticle production, often incorporate metals known for their potential health benefits, including gold, zinc, silver, selenium, palladium, and chromium [6,7]. The application of metallic nanoparticles across a diverse array of industries, such as biomedicine, agriculture, drug delivery, catalysis, antioxidant production, cytotoxicity, antibacterial and antibiofilm agents, as well as in the food industry and food packaging, has garnered significant attention. Moreover, metallic nanoparticles are utilized in various biotechnology, healthcare, and environmental remediation applications, including the mitigation of organic, inorganic, and radioactive pollution. Metallic nanoparticles, such as those made from gold, silver, platinum, palladium, zinc, cadmium sulfide, copper, iron, and titanium dioxide, exhibit exceptional antimicrobial properties, making them highly valuable across both industrial and biomedical sectors. Among these metallic nanoparticles, noble metals, particularly silver nanoparticles (AgNPs), occupy a central role due to their outstanding physicochemical properties. Recent research has intensified the investigation into these nanoparticles, highlighting their broad spectrum of applications. These include, but are not limited to, drug delivery, anticancer therapies, antioxidant functions, bactericidal and anti-inflammatory effects, wound healing, biological sensing, and biocatalytic activities [8,9]. Studies comparing the antibacterial activity of AgNPs, synthesized using various techniques, to that of commonly used antibiotics, consistently reveal that the nanoparticles demonstrate enhanced effectiveness. As such, silver nanoparticles show an increasingly significant function in both nanotechnology and nanomedicine. Their performance in combating antibiotic-resistant infections, along with their potential in advancing therapeutic interventions, underscores the growing significance of AgNPs within contemporary scientific and industrial research. In conclusion, the extensive range of applications and the unique properties of metallic nanoparticles, particularly silver nanoparticles, underscore their potential to drive innovation in numerous industries, including healthcare, agriculture, and environmental remediation. As research continues to evolve, the scope of these applications is expected to broaden, offering novel solutions to critical global challenges related to health, industry, and sustainability [10].

Activated carbon (AC) is a highly versatile material that possesses several desirable structural characteristics, including ease of use, safety, high adsorption capacity, a large surface area, and a microporous structure. In addition to these features, AC is considered an ideal material due to its abundance, low cost, and environmentally friendly nature. Furthermore, the presence of various functional groups, particularly those containing oxygen (O) and nitrogen (N), significantly influences the surface properties and chemical components of AC. These heteroatoms contribute to its high functionality and enhance its performance in various applications [11]. Despite its many advantages,

 doi:10.20944/preprints202505.1245.v1

activated carbon requires specialized treatment processes to address both chemical and microbiological concerns. Pure activated carbon is biocompatible; however, it has the potential to support bacterial growth under certain conditions. To overcome this issue, silver ions can be impregnated onto AC, resulting in silver-supported AC nanoparticles that exhibit enhanced antibacterial properties. The incorporation of silver nanoparticles onto activated carbon has generated considerable interest due to its broad range of applications, including catalysis, adsorption-desorption processes, and environmental purification, among others [12].

Magnetic nanoparticles are widely recognized for their exceptional biocompatibility, which makes them ideal for the modification of biomolecules [13]. In this study, the product obtained through green synthesis, using AC derived from the leaves of *Hibiscus esculentus* as a support material, was designated MIONPs/HEAC. The subsequent step involved investigating the binding characteristics of silver ions on the surface of the MIONPs/HEAC nanomaterials.

Hibiscus esculentus L. (generally known as okra) is native to Africa and belongs to the Malvaceae family. Okra is cultivated globally, particularly in tropical and temperate regions, including Southern Europe, the Middle East, Asia, and the Americas, for its nutritious unripe fruits. It is widely utilized for culinary purposes due to its nutritional value [14]. In addition to its fruit, the plants' seeds, flowers, leaves, and stems are utilized for their medicinal properties, offering notable pharmaceutical potential. The bioactive components in different plant parts vary, contributing to their diverse applications in the treatment of various ailments [15,16]. The peel, seeds, roots, fruits, and leaves of *Hibiscus esculentus* are rich in polyphenolic compounds, carotenoids, folic acid, oxalic acid, amino acids, oligomeric catechins, flavonol derivatives, as well as palmitic, oleic, and linoleic acids, carbohydrates, flavonol glycosides, minerals, and tannins. These compounds contribute to the plants' medicinal properties, including antioxidant, antimicrobial, and anti-inflammatory activities. As a result, *Hibiscus esculentus* holds great promise in the management of several diseases and health conditions [17]. Ongoing research continues to explore the full therapeutic potential of this plant, particularly regarding its role in the treatment of digestive disorders, diabetes, and possibly even its anti-cancer properties.

This research offers a widespread assessment of the antimicrobial activity of MIONPs/HEAC and MIONPs/HEAC@Ag nanoparticles against *S. aureus* ATCC 25923 and *E. coli* ATCC 25922. The antimicrobial performance of these synthesized nanomaterials was rigorously tested using two different methods, providing an in-depth understanding of their effectiveness as antimicrobial materials.

2. Materials and Methods

2.1. Chemicals

The analytically pure components, which were acquired from Sigma-Aldrich, include ferrous chloride tetrahydrate, ferric chloride hexahydrate, silver nitrate, sodium borate, hydrochloric acid, sodium hydroxide, ammonium hydrate, and zinc chloride. During the research, deionized water was used in the synthesis of the nanomaterial, preparation of the necessary solutions, and other processes.

2.2. Synthesis of HEAC

The *Hibiscus esculentus* fruits were initially rinsed with tap water and then cleaned 4-5 times with deionized water to eradicate any dust or contamination. After cleaning, the fruits were dehydrated at 25 °C temperature in a fume hood, ground using an IKA M20 Universal grinder, and stored for the preparation of HEAC. Ten grams of *Hibiscus esculentus* fruit powder were mixed with 250 mL of a 30 % zinc chloride solution in a 500 mL beaker and mixed at 80 °C for one hour. The obtained product was washed several times to remove impurities after being cooled in the laboratory, and then it was dried in a lyophilizer. The dried powder was then placed into a porcelain crucible and carbonized in a muffle furnace at 500 °C for 2 hours. After cooling to 25°C in a desiccator, the resulting HEAC was washed with 0.1 N hydrochloric acid to eliminate any remaining chlorine, zinc, and other ions. The

 doi:10.20944/preprints202505.1245.v1

obtained product was then rinsed with distilled water to neutralize its pH, lyophilized, and stored in a dark place for further synthesis and characterization [18,19].

2.3. Synthesis of MIONPs/HEAC

The synthesis of MIONPs coated with AC obtained from *HE* plant fruits was carried out with certain modifications to the protocol stated in the literature [20]. Initially, 1.5 g of iron(III) chloride hexahydrate was added to 25 mL of ultrapure water in a 50 mL three-neck flask and stirred at 25 °C temperature using a magnetic stirrer for 15 minutes. To prevent the hydrolysis of iron(III) ions, 2–3 drops of 37 % hydrochloric acid solution were added dropwise during stirring. Then, 1.05 g of iron(III) chloride tetrahydrate was added to the solution containing Fe^{3+} ions. The temperature was gradually increased to 90 °C and maintained under continuous magnetic stirring for 30 minutes. Subsequently, 10 mL of 26 % NH_3OH was added to the mixture, resulting in the formation of a black-colored product. The reaction solution was then mixed at the same temperature for an additional 30 minutes [13]. Then, 100 mL of water containing 0.5 g of AC from *HE* fruits was incorporated into the mixture. Stirring was maintained at 90 °C for an additional 60 minutes. After the reaction, the system was switched off and allowed to cool for 60 minutes. The formed MIONPs/HEAC nanoparticle solution was separated from the mixture using a neodymium magnet [13]. The product was washed 4-5 times with ultrapure water to remove any unreacted chemicals and then dried using a lyophilizer. The resulting MIONPs/HEAC nanoparticles were stored in a colored container for further characterization and experimental studies.

2.4. Synthesis of MIONPs/HEAC@Ag

To synthesize MIONPs/HEAC@Ag nanoparticles, 1 g of MIONPs/HEAC was ultrasonicated in 100 mL of ultrapure water. Then, 50 mL of 5 mM silver nitrate ($AgNO_3$) solution was added dropwise to the solution placed on a magnetic stirrer at 70 °C. Subsequently, this part of the mixture was stirred for an additional 60 minutes, and 0.6 grams of sodium borohydride ($NaBH_4$) was rapidly added while stirring to reduce Ag^+ ions to Ag^0. After the addition of $NaBH_4$, the mixture was stirred at 70 °C for 3 hours, leading to the formation of MIONPs/HEAC@Ag nanoparticles. The resulting nanoparticles were then separated from the solution using a neodymium magnet and cleaned 4–5 times with ultrapure water to eliminate any unreacted impurities [21,22]. The synthesis, characterization, and antimicrobial application mechanism of MIONPs/HEAC and MIONPs/HEAC@Ag nanoparticles are illustrated in Figure 1.

 doi:10.20944/preprints202505.1245.v1

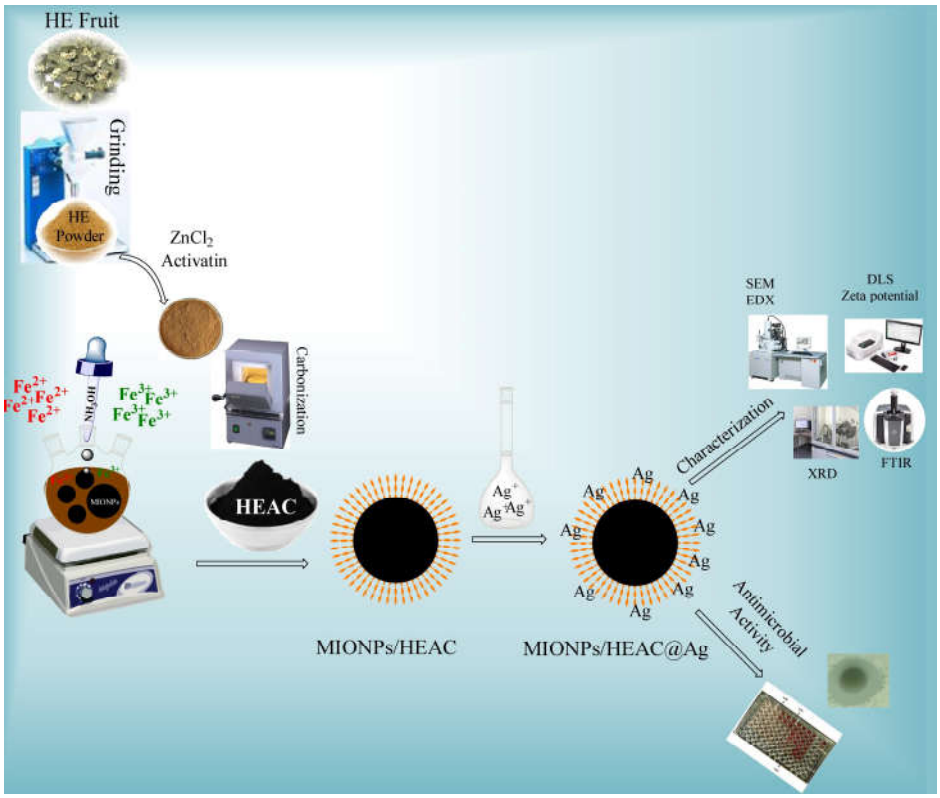

Figure 1. The synthesis, characterization, and antimicrobial application mechanism of MIONPs/HEAC and MIONPs/HEAC@Ag nanoparticles.

2.5. Nanoparticles characterization

Characterization of MIONPs/HEAC and MIONPs/HEAC@Ag nanoparticles was carried out using various techniques. XRD analysis was performed with a Rigaku RadB-Dmax II, while FTIR spectra were obtained using an Agilent Cary 630 FTIR spectrometer. SEM imaging was done with a LEO-EVO 40/Cambridge, and EDX analysis was conducted using a Bruker-125 eV/Berlin system. Particle size and zeta potential were conducted using a ZetaSizer Nano ZS90.

2.6. Analysis of antibacterial effect of MIONPs/HEAC and MIONPs/HEAC@Ag

The antimicrobial activity of MIONPs/HEAC and MIONPs/HEAC@Ag nanoparticles against *E. coli* and *S. aureus* was investigated using the microdilution and disk diffusion methods. Initially, bacterial cultures were grown in suitable media and incubated at 37 °C. Bacterial suspensions were adjusted to a concentration of $1.5x10^8$ CFU/mL, in accordance with the McFarland 0.5 turbidity standard. In the disc diffusion test, MIONPs/HEAC and MIONPs/HEAC@Ag nanoparticles were applied to sterile discs, which were then placed on Muller-Hinton agar plates that had been inoculated with the bacteria. Sterile ultrapure water was used as the positive control against the bacteria. The plates were incubated for 24 hours at 37 °C to allow bacterial growth and interaction with the nanoparticles. Following incubation, the zones of inhibition were measured in millimeters using a caliper. For the microdilution method, different concentrations of MIONPs/HEAC and MIONPs/HEAC@Ag nanoparticles were prepared by serial dilution using a micropipette. The antibiotics were diluted in the same manner for comparison purposes. Bacterial suspensions, prepared according to the McFarland 0.5 standard, were added to the wells of a microplate containing the nanoparticle dilutions. After incubation at 37 °C for 24 hours, a growth control was used to evaluate bacterial growth in the absence of nanoparticles. The minimum inhibitory concentration (MIC) was determined by measuring the lowest concentration of nanoparticles that inhibited

 doi:10.20944/preprints202505.1245.v1

bacterial growth. This experimental approach provides a comprehensive analysis of the antibacterial properties of MIONPs/HEAC and MIONPs/HEAC@Ag nanoparticles against *S. aureus* and *E. coli* by utilizing both disc diffusion and microdilution techniques [19].

3. Results and Discussion

3.1. Structural Characterization

3.1.1. FTIR Analysis

FTIR spectrometry was employed to investigate the synthesized HEAC, MIONPs/HEAC, and MIONPs/HEAC@Ag particles, with the results shown in Figure 2. In the FTIR spectra of the HEAC materials, a peak at 2113 cm^{-1} corresponds to the **C=C stretching vibration**, while a peak at 1990 cm^{-1} reveals the presence of the **C=C=C** allene structure, along with **–OH** and **C** groups at 1561 and 1401 cm^{-1}. A peak at 1036 cm^{-1} is attributed to **C-N stretching** and **–H bending vibrations**. For the MIONPs/HEAC nanoparticles, an absorbance peak at **3365 cm^{-1}** is related to the **–OH stretching vibrations** of phenolic and alcoholic groups. When polysaccharides were incorporated into the MIONPs/HEAC@Ag nanoparticle, faint peaks at **2922 cm^{-1}** appeared, indicating **C–H stretching** from **CH, CH_2, and CH_3** groups. Examining the spectra of MIONPs/HEAC and MIONPs/HEAC@Ag nanoparticles, peaks at **2109 cm^{-1}, 2113 cm^{-1}**, and **1990 cm^{-1}** signify the presence of **alkyne** and **C-H groups**. The **carbonyl (C=O)** peaks detected at **1636 cm^{-1}** and **1654 cm^{-1}** are linked to the presence of **carboxylic acid** and **hydroxyl** moieties, common in polyphenols, phenolic acids, and proteins. Furthermore, peaks at **1401 cm^{-1}** reflect **–OH and C-H bending vibrations**, and those at **1039 cm^{-1}** and **1077 cm^{-1}** indicate the presence of **C-O** and **C-N groups**. Lastly, a peak at **536 cm^{-1}** in the spectra of MIONPs/HEAC and MIONPs/HEAC@Ag nanoparticles confirms the existence of the **Fe-O bond [13,18,19].**

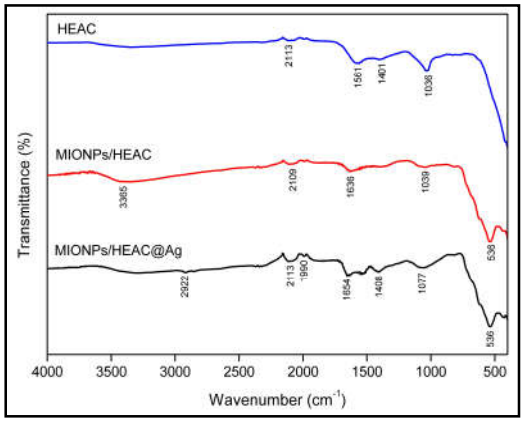

Figure 2. FTIR spectra of HEAC, MIONPs/HEAC, and MIONPs/HEAC@Ag.

3.1.2. SEM Analysis

The surface characteristics of MIONPs/HEAC and MIONPs/HEAC@Ag nanoparticles were investigated using SEM. Figure 3a,b present the SEM images of MIONPs/HEAC and MIONPs/HEAC@Ag nanoparticles, respectively.

 doi:10.20944/preprints202505.1245.v1

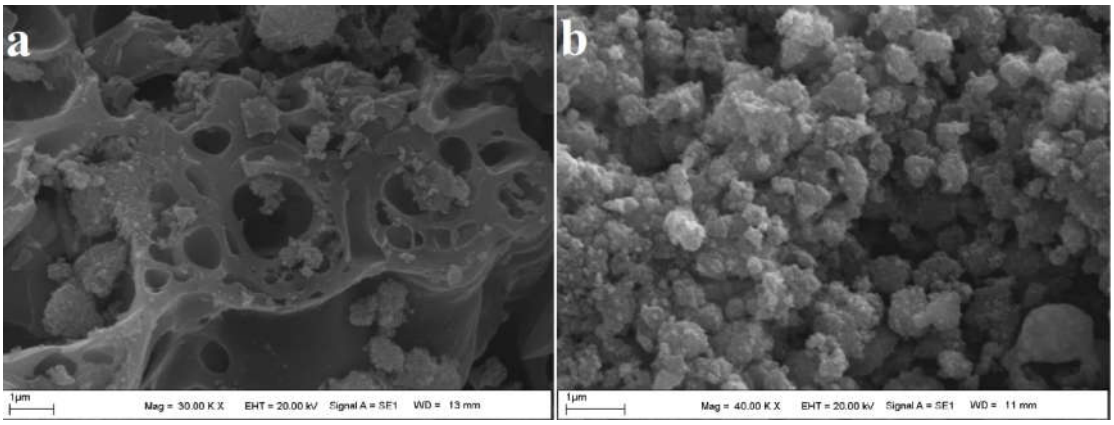

Figure 3. SEM images of (a) MIONPs/HEAC; (b) MIONPs/HEAC@Ag.

The MIONPs/HEAC nanoparticles exhibit a granular surface with pores of varying diameters, indicative of a heterogeneous and porous morphology. In contrast, significant alterations in surface topology are observed upon the incorporation of silver (Ag) ions onto the MIONPs/HEAC surface, forming MIONPs/HEAC@Ag nanoparticles. The surface of the MIONPs/HEAC@Ag nanoparticles appears considerably smoother, suggesting a more homogeneous distribution of Ag^0 across the surface. This smoothening effect is likely due to the interaction between Ag^0 and the surface of the MIONPs/HEAC, which reduces its surface irregularities. The observed changes in both the pore architecture and surface morphology underscore the impact of Ag^0 attachment on the structural properties of the nanoparticles [23,24].

3.2.3. EDX Analysis

The surface components of MIONPs/HEAC and MIONPs/HEAC@Ag nanoparticles were characterized using EDX analysis. Figure 4 presents the EDX spectra of both MIONPs/HEAC and MIONPs/HEAC@Ag nanoparticles.

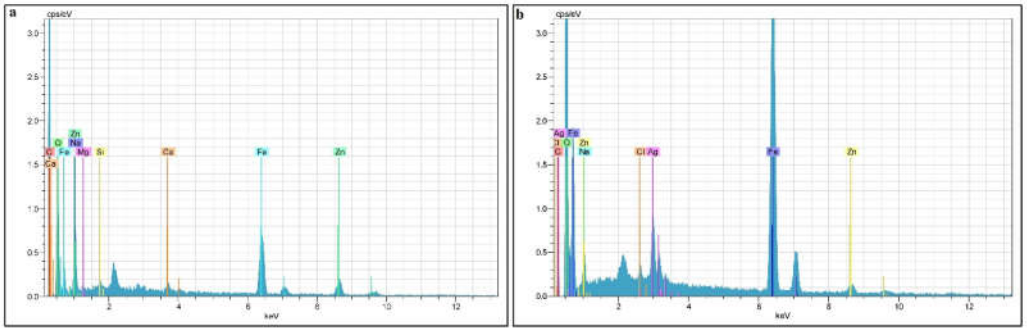

Figure 4. EDX images of (a) MIONPs/HEAC; (b) MIONPs/HEAC@Ag.

The EDX analysis of MIONPs/HEAC nanoparticles revealed the presence of iron (Fe), oxygen (O), carbon (C), and zinc (Zn), which are critical elements in the composition. In contrast, the EDX spectrum of MIONPs/HEAC@Ag nanoparticles additionally detected silver (Ag), confirming its incorporation into the nanoparticle structure. This analysis verifies the presence of iron and silver in both MIONPs/HEAC and MIONPs/HEAC@Ag nanoparticles, as shown in Figure 4a,b [25].

 doi:10.20944/preprints202505.1245.v1

3.2.4. DLS Analysis

The results of the DLS analysis, conducted after sonicating and suspending 5 mg of MIONPs/HEAC and MIONPs/HEAC@Ag nanoparticles in 50 mL of ultrapure water, are presented in Figure 5. DLS analysis is an effective method for determining the particle size distribution within a solid-liquid suspension. Upon examination of the DLS data, it is observed that the average particle size of MIONPs/HEAC is 122 nm, while the average particle size of MIONPs/HEAC@Ag is 164 nm. This increase in size is in comparison to the size distribution of silver nanoparticles as reported in previous studies [13,19].

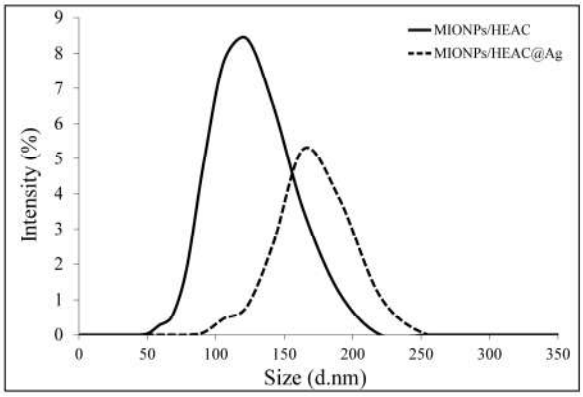

Figure 5. DLS diagram of MIONPs/HEAC and MIONPs/HEAC@Ag.

3.2.5. Zeta Potential Analysis

Figure 6 presents the results of the zeta potential investigation conducted on nanoparticles comprising MIONPs/HEAC and MIONPs/HEAC@Ag. The zeta potential serves as an indicator of the surface charge of a material, which is crucial for assessing the stability of nanoparticle suspensions. To ensure minimal agglomeration and clustering, it is necessary to achieve zeta potential values that are sufficiently positive or negative. The zeta potential values recorded for MIONPs/HEAC and MIONPs/HEAC@Ag nanoparticles were -16.8 mV and -16.3 mV, respectively, under optimal conditions for performance. These values suggest that both types of nanoparticles exhibit minimal agglomeration tendencies and maintain suspension stability over extended periods. Consequently, the suspensions of MIONPs/HEAC and MIONPs/HEAC@Ag remain stable for several months, confirming the effectiveness of their preparation and dispersion [18,19].

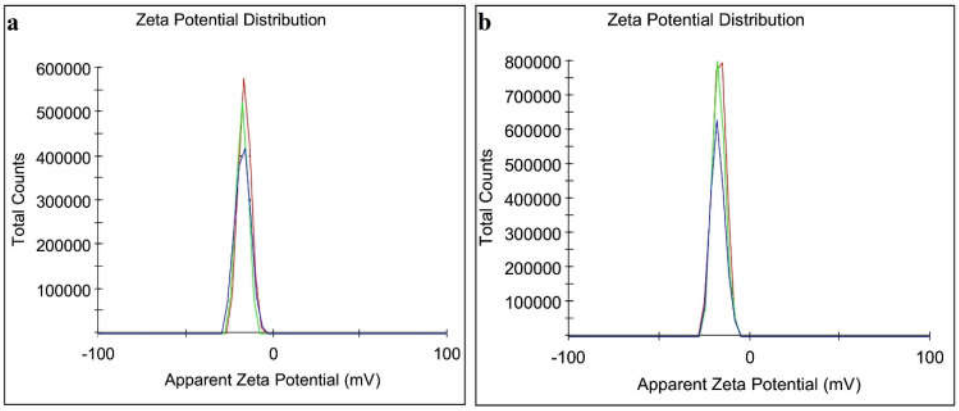

Figure 6. Zeta potential diagram of (a) MIONPs/HEAC, (b) MIONPs/HEAC@Ag.

 doi:10.20944/preprints202505.1245.v1

3.2.6. XRD Analysis

Figure 7 presents the XRD pattern used to investigate and compare the crystal phases of MIONPs/HEAC and MIONPs/HEAC@Ag nanoparticles.

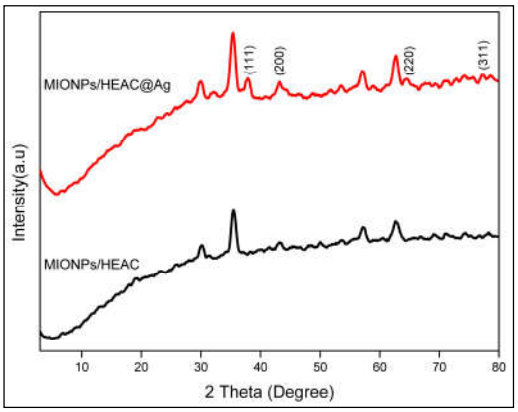

Figure 7. XRD images of MIONPs/HEAC and MIONPs/HEAC@Ag.

The diffraction peaks observed at 2θ values corresponding to (111), (200), (220), and (311) reflections are characteristic of both MIONPs/HEAC and MIONPs/HEAC@Ag nanoparticles. The XRD pattern for MIONPs/HEAC exhibited peaks consistent with the JCPDS card number 65-3107, while the pattern for MIONPs/HEAC@Ag corresponded to JCPDS card number 49-1287. The values obtained from the measurements are consistent with those reported in the literature, confirming the successful formation of the synthesized nanoparticle phases. The crystallite sizes of MIONPs/HEAC and MIONPs/HEAC@Ag were calculated using the Debye-Scherrer equation, yielding values of 21.85 nm and 22.40 nm, respectively. These values were derived from the highest intensity peaks at 2θ values of 35.440° and 35.500°. The slight increase in crystallite size in MIONPs/HEAC@Ag compared to MIONPs/HEAC suggests the incorporation of silver does not significantly alter the overall crystal structure, but leads to a modest increase in particle size. In conclusion, the XRD data confirm that both MIONPs/HEAC and MIONPs/HEAC@Ag nanoparticles were successfully synthesized, with distinct crystalline structures and sizes. The incorporation of silver in the MIONPs/HEAC composite was verified without significant distortion of the crystalline phase [13,18,19].

3.2. Antibacterial properties of MIONPs/HEAC and MIONPs/HEAC@Ag

The antibacterial properties of MIONPs/HEAC and MIONPs/HEAC@Ag nanoparticles were evaluated through disc diffusion and microdilution assays. The results presented in Table 1 reveal that the MIONPs/HEAC@Ag nanoparticle had a notable antibacterial effect on two bacterial species (*S. aureus* and *E. coli*). The MIONPs/HEAC@Ag nanoparticles exhibited greater antibacterial activity against the gram-positive *S. aureus* at lower concentrations in the microdilution assay, compared to their activity against the gram-negative *E. coli*. These results were in agreement with the disc diffusion findings, as shown in Table 1. The observed variation may be attributed to the structural differences between gram-positive and gram-negative bacteria [28].

The cell wall of gram-positive bacteria, such as *S. aureus*, is composed of a thick peptidoglycan layer, which is essential for maintaining the structural integrity of the cell. This peptidoglycan network is cross-linked by small peptides, forming a robust and extensive structure. In contrast, gram-negative bacteria, such as *E. coli*, have a more complex cell wall architecture, which includes an outer membrane containing lipopolysaccharides. This additional layer acts as a barrier, limiting the penetration of external agents, including nanoparticles. Consequently, the structural complexity of gram-negative bacteria results in a reduced susceptibility to the MIONPs/HEAC@Ag nanoparticles compared to gram-positive bacteria. The variations in bacterial cell wall structures help to clarify why the MIONPs/HEAC@Ag nanoparticles exhibit greater antibacterial activity against *S. aureus* than *E.*

 doi:10.20944/preprints202505.1245.v1

coli. The findings highlight the potential of these nanoparticles as effective antibacterial agents, particularly for targeting gram-positive bacterial infections [29,30].

Table 1. *S. aureus* strains were tested with colistin, and *E. coli* strains with vancomycin for comparative study.

Microorganism	Dilution Method (µg/mL)			Disc Method Zone of Inhibition (mm)		
				Control Disc		
	Antibiotic	MIONPs/HEAC	MIONPs/HEAC@Ag	Deionized water	MIONPs/HEAC	MIONPs/HEAC@Ag
E. coli	2.0	96	3.0	0.0	0.0	11.50
S. aureus	1.0	48	1.5	0.0	0.0	13.00

Metallic nanoparticles are highly valued for their diverse range of applications, particularly in the field of antimicrobial research, and are continually being optimized for enhanced effectiveness. Among these, silver ions are widely recognized for their antimicrobial properties. When silver ions are either ionized or diffuse into their environment, they exhibit heightened reactivity. These ions are drawn to microorganisms through electrostatic forces, where they interact with the microbial cells. The interaction of silver ions with bacteria leads to the formation of Reactive Oxygen Species (ROS), which are chemically reactive molecules that induce oxidative stress. This oxidative stress disrupts the integrity of the microbial cell membrane, resulting in structural damage and impairment of cellular functions. Additionally, ROS interacts with key macromolecules, including RNA, DNA, and enzymes, compromising their structure and function. The sensitivity of RNA to ROS further contributes to the destabilization of the microbial cell, as it interferes with essential macromolecular processes. This disruption ultimately leads to the inability of the microorganisms to maintain proper growth and survival, resulting in cell death [31–36].

Figure 8 demonstrates the antibacterial activity of MIONPs/HEAC@Ag against *E. coli* and *S. aureus*. The observed antibacterial effect is primarily attributed to the disruption of the bacterial membrane integrity and function. This disruption results from the interference with essential cellular mechanisms, including the generation of ROS, inhibition of protein synthesis, and damage to the bacterial DNA structure. Ultimately, these disturbances culminate in the death of the microorganisms. The silver component incorporated into the MIONPs/HEAC@Ag composite is believed to play a pivotal role in mediating these antimicrobial effects.

 doi:10.20944/preprints202505.1245.v1

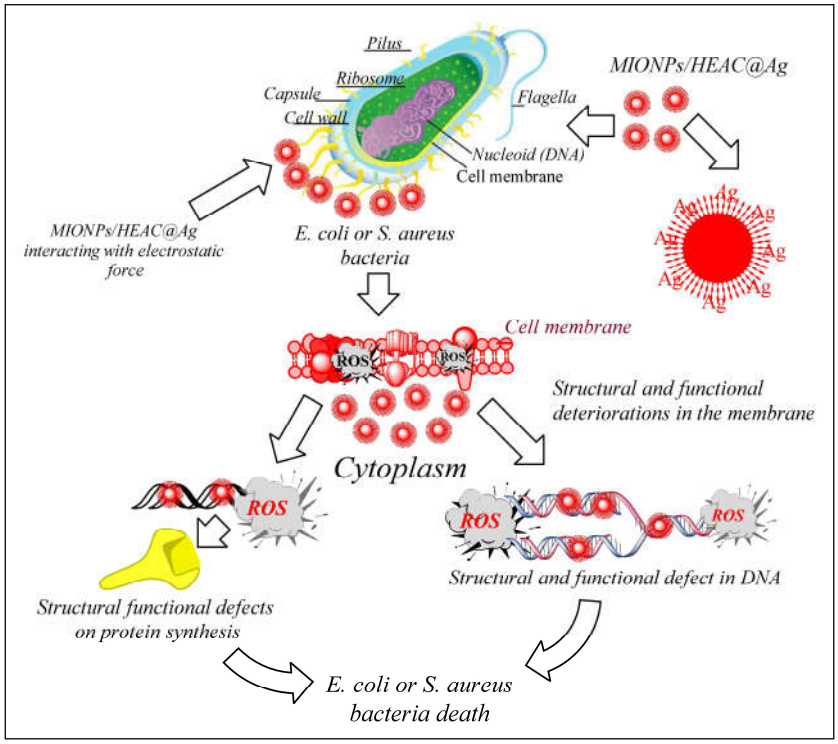

Figure 8. Representative scheme of antimicrobial activity of MIONPs/HEAC@Ag nanoparticles.

4. Conclusions

The MIONPs/HEAC@Ag nanoparticles were synthesized by binding activated carbon (AC) derived from the fruits of *Hibiscus esculentus* to magnetic iron oxide nanoparticles (MIONPs), which were prepared using the co-precipitation method. Subsequently, silver (Ag) ions were incorporated onto these nanoparticles. Notably, no oxidation occurred during the synthesis of both MIONPs/HEAC and MIONPs/HEAC@Ag nanoparticles. The presence of AC and Ag in the nanoparticle structure was confirmed through XRD and FTIR analyses. Furthermore, the saturation magnetization of the MIONPs was found to decrease upon the incorporation of AC and Ag, indicating the influence of these components on the magnetic properties of the nanoparticles. Both MIONPs/HEAC and MIONPs/HEAC@Ag nanoparticles exhibited antibacterial activity against *S. aureus* and *E. coli*. However, MIONPs/HEAC@Ag nanoparticles demonstrated enhanced antimicrobial efficacy, likely due to the combined effects of the magnetic properties and the bactericidal activity of Ag. In conclusion, MIONPs/HEAC and MIONPs/HEAC@Ag nanoparticles have shown promising potential as antibacterial agents and could be utilized in applications requiring effective bacterial inhibition.

Author Contributions: Conceptualization, M.G. and E.E.; methodology, E.E. and S.T.; software, P.Z.; validation, F.N., T.K., O.S.; formal analysis, Y.K. and P.G.; investigation, M.G., E.E., S.T., P.Z., F.N., T.K., Y.K., O.Š., O.S., P.G., D.G.; resources, M.G., E.E., T.K., O.S.; data curation, E.E., T.K., O.S.; writing—original draft preparation, M.G., E.E., S.T., P.Z., F.N., T.K., O.S., D.G.; writing—review and editing, T.K., O.Š., O.S., D.G., A.K.; visualization, T.K., O.S., A.K.; supervision, E.E., T.K., O.S.; project administration, E.E., T.K., O.S.; funding acquisition, E.E., T.K., O.S. All authors have read and agreed to the published version of the manuscript.

Data Availability Statement: Data are available on request.

Acknowledgments: This work was supported in part by the Ministry of Education and Science of Ukraine (projects Nos. 0122U000850, 0122U000874, 0125U001054, 0125U002005, and 0125U002033), National Research Foundation of Ukraine (project No. 2020.02/0100), Slovak Grant Agency VEGA (projects Nos. 2/0166/22 and

 doi:10.20944/preprints202505.1245.v1

2/0131/25), and Slovak Research and Development Agency (project No. APVV-21-0335). T.K. and Y.K. also acknowledge the SAIA (Slovak Academic Information Agency) for scholarships in the Institute of Physics of the Slovak Academy of Sciences in the framework of the National Scholarship Programme of the Slovak Republic. This work has also received funding through the MSCA4Ukraine project (grant No. 1128327), which is funded by the European Union. O.S. acknowledges US National Science Foundation (NSF) grant CBET-2235349, including IMPRESS-U supplement, and NSF-BSF grant CBET-2422672.

Conflicts of Interest: The authors declare no conflicts of interest.

References

1. Das, A.; Sengupta, P.; Chatterjee, S.; Khanam, J.; Mondal, P.K.; Romero, E.L.; Ghosal, K. Development and Evaluation of Magnetite Loaded Alginate Beads Based Nanocomposite for Enhanced Targeted Analgesic Drug Delivery. *Magnetochemistry*, **2025**, *11*(2), 14.
2. Attar, S.R.; Sapkal, A.C.; Bagade, C.S.; Ghanwat, V. B.; Kamble, S.B. Biogenic CuO NPs for synthesis of coumarin derivatives in hydrotropic aqueous medium. *Res. Chem. Intermed*. **2023**, *49*(7), 2989-3004.
3. Adeeyo, A.O.; Alabi, M.A.; Oyetade, J.A.; Nkambule, T.T.; Mamba, B.B.; Oladipo, A.O.; Msagati, T.A. Magnetic Nanoparticles: Advances in Synthesis, Sensing, and Theragnostic Applications. *Magnetochemistry*, **2025**, *11*(2), 9.
4. Fadeel, B. Nanomaterial characterization: Understanding nano-bio interactions. *Biochem. Biophys. Res. Commun*. **2022**, *633*, 45-51.
5. Ariga, K.; Fakhrullin, R. Nanoarchitectonics in Materials Science: Method for Everything in Materials Science. *Materials* **2023**, *16*(19), 6367.
6. Bataineh, S.M.; Arafa, I.M.; Abu-Zreg, S.M.; Al-Gharaibeh, M.M.; Hammouri, H.M.; Tarazi, Y.H.; Darmani, H. Synergistic effect of magnetic iron oxide nanoparticles with medicinal plant extracts against resistant bacterial strains. *Magnetochemistry*, **2024**, *10*(7), 49.
7. De, A.; Singh, N.B.; Guin, M.; Barthwal, S. Water purification by green synthesized nanomaterials. *Curr. Pharm. Biotechnol*. **2023**, *24*(1), 101-117.
8. Wahab, M.A.; Li, L.; Li, H.; Abdala, A. Silver nanoparticle-based nanocomposites for combating infectious pathogens: Recent advances and future prospects. *Nanomater*. **2021**, *11*(3), 581.
9. Begum, S.J.; Pratibha, S.; Rawat, J.M.; Venugopal, D.; Sahu, P.; Gowda, A.; Jaremko, M. Recent advances in green synthesis, characterization, and applications of bioactive metallic nanoparticles. *Pharm*. **2022**, *15*(4), 455.
10. Alburae, N.; Alshamrani, R.; Mohammed, A.E. Bioactive silver nanoparticles fabricated using *Lasiurus scindicus* and *Panicum turgidum* seed extracts: Anticancer and antibacterial efficiency. *Sci. Rep.* **2024,** *14*(1), 4162.
11. Lobato-Peralta, D.R.; Duque-Brito,E.; Ayala-Cortés, A.; Arias,D.M.; Longoria,A.; Cuentas-Gallegos, A.K.; Okoye, P.U.: Advances in activated carbon modification, surface heteroatom configuration, reactor strategies, and regeneration methods for enhanced wastewater treatment. *J. Environ. Chem. Eng*. **2021**, *9*(4), 105626.
12. Kang, N.; Fan, Y.; Li, D.; Jia, X.; Zhao, S. Preparation of Magnetic Nano-Catalyst Containing Schiff Base Unit and Its Application in the Chemical Fixation of CO_2 into Cyclic Carbonates. *Magnetochemistry*, **2024**, *10*(5), 33.
13. Doğan, Y.; Öziç, C.; Ertaş, E.; Baran, A.; Rosic, G.; Selakovic, D.; Eftekhari, A. Activated carbon-coated iron oxide magnetic nanocomposite (IONPs@CtAC) loaded with morin hydrate for drug-delivery applications. *Front. Chem*. **2024**, *12*, 1477724.
14. Zhu, X.M.; Xu, R.; Wang, H.; Chen, J.Y.; Tu, Z.C. Structural properties, bioactivities, and applications of polysaccharides from Okra [*Abelmoschus esculentus* (L.) Moench]: A review. *J. Agric. Food Chem*. **2020**, *68*(48) 14091-14103.
15. Elkhalifa, A.E.O.; Alshammari, E.; Adnan, M.; Alcantara, J.C.; Awadelkareem, A.M.; Eltoum, N.E.; Ashraf, S.A. Okra (*Abelmoschus esculentus*) as a potential dietary medicine with nutraceutical importance for sustainable health applications. *Molecules* **2021**, *26*(3), 696.

 doi:10.20944/preprints202505.1245.v1

16. Deen, G.R.; Hannan, F.A.; Henari, F.; Akhtar, S. Effects of different parts of the okra plant (*Abelmoschus esculentus*) on the phytosynthesis of silver nanoparticles: evaluation of synthesis conditions, nonlinear optical and antibacterial properties. *Nanomater*. **2022**, *12*(23), 4174.
17. Agregán, R.; Pateiro, M.; Bohrer, B.M.; Shariati, M.A.; Nawaz, A.; Gohari, G.; Lorenzo, J.M. Biological activity and development of functional foods fortified with okra (*Abelmoschus esculentus*). *Crit. Rev. Food Sci. Nutr*. **2023**, *63*(23), 6018-6033.
18. Öziç, C.; Ertaş, E.; Baran, M.F.; Baran, A.; Ahmadian, E.; Eftekhari, A.; Yıldıztekin, M. Synthesis and characterization of activated carbon-supported magnetic nanocomposite (MNPs-OLAC) obtained from okra leaves as a nanocarrier for targeted delivery of morin hydrate. *Front. Pharmacol*. **2024**, *15*, 1482130.
19. Baran, A.; Ertaş, E.; Baran, M.F.; Eftekhari, A.; Gunes, Z.; Keskin, C.; Khalilov, R. Green-Synthesized characterization, antioxidant and antibacterial applications of CtAC/MNPs-Ag nanocomposites. *Pharm*. **2024**, *17*(6), 772.
20. Deivayanai, V.C.; Karishma, S.; Thamarai, P.; Saravanan, A.; Yaashikaa, P.R. Artificial neural network modeling of dye adsorption kinetics and thermodynamics with magnetic nanoparticle-activated carbon from *Allium cepa* peels. *Chem. Pap*. **2025**, 79, 1775-1796.
21. Chishti, A.N.; Guo, F.; Aftab, A.; Ma, Z.; Liu, Y.; Chen, M.; Diao, G. Synthesis of silver doped Fe_3O_4/C nanoparticles and its catalytic activities for the degradation and reduction of methylene blue and 4-nitrophenol. *Appl. Surf. Sci*. **2021**, *546*, 149070.
22. Atunwa, B.T.; Dada, A.O.; Inyinbor, A.A.; Pal, U. Synthesis, physiochemical and spectroscopic characterization of *Palm kernel* shell activated carbon doped AgNPs (PKSAC@AgNPs) for adsorption of chloroquine pharma-ceutical waste. *Mater. Today: Proc*. **2022**, *65*, 3538-3546.
23. Moazzen, M.; Khaneghah, A.M.; Shariatifar, N.; Ahmadloo, M.; Eş, I.; Baghani,A.N.; Khaniki,G.J. Multi-walled carbon nanotubes modified with iron oxide and silver nanoparticles (MWCNT-Fe_3O_4/Ag) as a novel adsorbent for determining PAEs in carbonated soft drinks using magnetic SPE-GC/MS method. *Arab. J. Chem*. **2019**, *12*(4), 476-488.
24. Foroutan, R.; Peighambardoust, S.J.; Peighambardoust, S.H.; Pateiro, M.; Lorenzo, J.M.: Adsorption of crystal violet dye using activated carbon of lemon wood and activated carbon/Fe_3O_4 magnetic nanocomposite from aqueous solutions: a kinetic, equilibrium and thermodynamic study. *Molecules* **2021**, *26*(8), 2241.
25. Lee, H.; Park, J.; Park, Y.K.; Kim, B.J.; An, K.H.; Kim, S.C.; Jung, S.C.: Preparation and characterization of silver-iron bimetallic nanoparticles on activated carbon using plasma in liquid process. *Nanomat*. **2021**, *11*(12), 3385.
26. Wang, Z.; Xu, W.; Jie, F.; Zhao, Z.; Zhou, K.; Liu, H.: The selective adsorption performance and mechanism of multiwall magnetic carbon nanotubes for heavy metals in wastewater. *Sci. Rep*. **2021**, *11*, 16878.
27. Sepahvand, S.; Farhadi, S. Fullerene-modified magnetic silver phosphate (Ag_3PO_4/Fe_3O_4/C_{60}) nanocomposites: Hydrothermal synthesis, charac- terization and study of photocatalytic, catalytic and antibacterial activities. *RSC Adv*. **2018**, *8*(18), 10124-10140.
28. Arain, M.B.; Yilmaz, E.; Hoda, N.; Kazi, T.G.; Soylak, M. Magnetic solid-phase extraction of quercetin on magnetic-activated carbon cloth (MACC). *J. Iran. Chem. Soc.* **2019**, *16*, 1365-1372.
29. Patil, M.P.; Singh, R.D.; Koli, P.B.; Patil, K.T.; Jagdale, B.S.; Tipare, A.R.; Kim, G.D. Antibacterial potential of silver nanoparticles synthesized using *Madhuca Longifolia* flower extract as a green resource. *Microb. Pathog*. **2018**, *121*, 184-189.
30. Yan, C.; Wang, C.; Hou, T.; Guan, P.; Qiao, Y.; Guo, L.; Wu, H. Lasting tracking and rapid discrimination of live gram-positive bacteria by peptidoglycan-targeting carbon quantum dots. *ACS Appl. Mater. Interfaces*. **2021**, *13*(1), 1277-1287.
31. Tavares, T.D.; Antunes, J.C.; Padrão, J.; Ribeiro, A.I.; Zille, A.; Amorim, M.T.P.; Felgueiras, H.P. Activity of specialized biomolecules against gram- positive and gram-negative bacteria. *Antibiotics* **2020**, *9*(6), 314.
32. Alav, I.; Kobylka, J.; Kuth, M.S.; Pos, K.M.; Picard, M.; Blair, J.M.; Bavro, V.N.: Structure, assembly, and function of tripartite efflux and type 1 secretion systems in gram-negative bacteria. *Chem. Rev.* **2021**, *121*(9), 5479-5596.

 doi:10.20944/preprints202505.1245.v1

33. Tural, B.; Ertaş, E.; Batıbay, H.; Tural, S. The Impact of *Pistacia khinjuk* plant gender on silver nanoparticle synthesis: Are extracts of root obtained from female plants preferentially used? *Biochem. Biophys. Res. Commun*. **2025**, *746*, 151257.
34. Adeniji, O.O.; Ojemaye, M.O.; Okoh, A.I.: Antibacterial activity of metallic nanoparticles against multidrug-resistant pathogens isolated from environmental samples: nanoparticles/antibiotic combination therapy and cytotoxicity study. *ACS Appl. Bio Mater.* **2022**, *5*(10), 4814-4826.
35. Tural, B.; Ertaş, E.; Batıbay, H.; Tural, S. Comparative Study on Silver Nanoparticle Synthesis Using Male and Female *Pistacia Khinjuk* Leaf Extracts: Enhanced Efficacy of Female Leaf Extracts. *ChemistrySelect* **2024**, *9*(30), e202402117.
36. Castrillon, E.D.C.; Correa, S.; Ávila-Torres, Y.P. Impact of Magnetic Field on ROS Generation in Cu-g-C3N4 Against *E. coli* Disinfection Process. *Magnetochemistry*, **2025**, *11*(4), 28.